Supplementary Materials

The effect of sample size on the predictability and reliability of CCM

The applicability of CCM can be affected by the sample size of data, as the predictability of causal interactions increases with the increasing sample size (Sugihara, et al., 2012). Here, we performed two analyses to examine the sample size effect on the predictability and reliability of CCM in fMRI data.

Predictability of CCM in simulated data. First, we investigated the sample size effect on the predictability of CCM based on the simulated data. We simulated a nonlinear dynamical system containing two coupled difference equations that exhibit chaotic behaviors, as demonstrated by Sugihara, et al. (2012):

$$X(t+1) = X(t)[r_x - r_x X(t) - \beta_{x,y} Y(t)]$$

$$Y(t+1) = Y(t)[r_y - r_y X(t) - \beta_{y,x} X(t)]$$

where r_x = 3.8, r_y = 3.5, $\beta_{x,y}$ = 0.002, and $\beta_{y,x}$ = 0.1. The initial states of $X(0)$ and $Y(0)$ were randomly chosen from the standard uniform distribution with the interval (0,1). In this system, variable *X* exerted the causal influence on variable *Y*, while considerably weak vice versa. Using this model, we simulated 1200 time points raw signals of both *X* and *Y* and simply assumed that the simulated time series represented the underlying neural activities of two brain regions. Then, the Balloon–Windkessel hemodynamic model was applied on the raw signals to generate corresponding BOLD signals (Buxton, et al., 1998; Friston, et al., 2000). Parameters in the model (e.g., the signal decay, transit time, echo time, etc.) were assigned as default values in the fMRI Simulation Toolbox (SimTB) (Erhardt, et al., 2012). Finally, the first 200 time points of the resultant time series were discarded to enable variables achieve stable dynamics. The causality between *X* and *Y* was calculated by implementing CCM on the raw time series and simulated BOLD signals, separately. The length of time series was selected as a range of 50-

1000 time points with steps of 50 to investigate the sample size effect on the predictability. The whole simulation and estimation process were repeated for 100 times.

For both types of time series (e.g., the raw time series and simulated BOLD signals), we found that the average causality coefficients of *X* to *Y* were much larger than *Y* to *X* (around zero), indicating the credible predictability for the causal direction of CCM. Meanwhile, the causality coefficients of *X* to *Y* were the higher for the raw time series than the simulated BOLD signals, suggesting that the hemodynamic response can affect the predictability of CCM. Moreover, we found that the causality coefficient tended to remain stably above 0.8 for raw time series and 0.6 for simulated BOLD signals when sample size is larger than 200, suggesting a reliable predictability of CCM in detecting causal relationship with sample size larger than 200 (Fig. S5).

Reliability of CCM in real data. To estimate the sample size effect on the reliability of CCM, we constructed the directed functional networks with different signal length for each individual and calculated the intra-class correlation coefficient (*ICC*) for each connection. Briefly, based on the preprocessed data, we constructed the directed functional networks with the first 100, 150, 200, 250 and 300 time points for each individual, respectively. Then, the *ICC* for each connection was calculated between each network constructed with cut time series and the network constructed with the full time series length (i.e., 365), using the following formula (Shrout and Fleiss, 1979):

$$ICC = (\sigma_{bs}^2 - \sigma_{ws}^2)/[\sigma_{bs}^2 + (m-1)\sigma_{ws}^2]$$

where σ_{bs} is the between-subject variance, σ_{ws} is the within subject variance, and m is the number of repeated measures. Thus, we obtained an *ICC* map for each time point segment, which represents the reliability to the network constructed with full time series length. Notably, *ICC* is a normalized measure which has a maximum of 1. The *ICC* values were commonly categorized into five intervals (Landis and

Koch, 1977): $0 < ICC \leq 0.2$ (slight), $0.2 < ICC \leq 0.4$ (fair), $0.4 < ICC \leq 0.6$ (moderate), $0.6 < ICC \leq 0.8$ (substantial), and $0.8 < ICC \leq 1.0$ (almost perfect).

In general, the reliability of CCM increases with increasing sample size and the average ICCs reached 0.457, 0.596, 0.730, 0.827 and 0.910 for 100, 150, 200, 250 and 300 time points, respectively. These results suggest the moderate to perfect reliability of CCM in constructing directed functional networks from real BOLD data, even with a sample size less than 300. (Figure S6).

The effect of dimension *E* in CCM on network construction

In our main analysis, we set the reconstructing dimension $E = 3$ according to analyses on the ratio of false neighbors (Kennel, et al., 1992). Here, we further investigated whether the selection of reconstructing dimension *E* on CCM could affect the construction of the directed functional brain networks. We chose different *E* levels, e.g., $E = 3$, 5, 7, 9 and 11, and redid the causality coefficients estimation between every two nodes by using CCM, separately. Accordingly, a 160×160 causality coefficients matrix was obtained at each level of *E* for each subject. Next, we calculated the *ICC* scores across different *E* levels for each connection within the network to assess the reliability of directed functional network construction under different *E* levels.

The result showed that 30.7% of the connections exhibited an excellent reliability of $ICC > 0.8$, and 96.9% connections had at least moderate reliability of $ICC > 0.4$. These results suggested that the construction of the directed functional network retained stable among different selection of the parameter *E* in CCM.

Effect of network construction with random projection method

The use of the standard delay-coordinate in CCM might decrease the predictability when estimating causal relationship in a highly heterogeneous system with high dimensionality, and a plenty of data samples are thus required to maintain the high predictability in CCM (Tajima, et al., 2015). To reduce the dimensionality of data, a random projection method was proposed by Tajima, et al. (2015). Here, we employed this method in network construction procedures and re-performed the analyses to examine whether our main results were sensitive to the mapping algorithm. In detail, when constructing the phase-shifted space, we projected the delay vector (i.e., the reconstructed variable), $\underline{x}(t) = [x(t\text{-}T), x(t\text{-}2T), \ldots, x(t\text{-}(E\text{-}1)T)]$, to a randomized coordinate space by multiplying a square random matrix, $\boldsymbol{R}$, from the left of $\underline{x}(t)$ to obtain a transformed vector: $\underline{x}_d(t) = \boldsymbol{R}\underline{x}(t)$. The random matrix was generated from the Gaussian distribution centered at zero with the standard deviation of one. The randomized vector $\underline{x}_d(t)$, instead of $\underline{x}(t)$, was used for following steps of causality estimation. Then, we performed the same analysis protocol as those in the main text.

We found the resultant causality coefficient matrix was highly similar to the one constructed by the standard CCM algorithm, indicated by a spatial correlation of $r = 0.98$ between the group-level matrices. The network also exhibited a small-world architecture, with $\sigma = 1.64$, $\gamma = 1.71$ and $\lambda = 1.04$. Moreover, the network demonstrated highly similar motif patterns with our main findings that there were 1397 unidirected motifs and 1425 reciprocal motifs, three-node motif ID = 4, 6, 9, 12 and 13 were identified with significantly great frequencies ($Z > 1.96$), and the three-node motif profiles were almost same with the standard one ($r = 0.997$). Together, these results suggest our findings are robust to the dimensionality reduction method.

Hubs in directed functional brain networks constructed by Granger causality analysis

To compare the hub set between networks constructed using CCM and Granger Causality (GC), we used the GC method to construct the directed functional brain networks and identified their hubs. The code of GC was downloaded from https://www.mathworks.com/matlabcentral/fileexchange/25467-granger-causality-test, which is based on the original GC definition (Granger, 1969), and uses Bayesian information criterion to determine the lag length. For each subject, the F-statistic value was calculated by performing GC test between every two nodes. Consequently, a 160×160 F-statistic matrix was obtained for each subject and the group-level GC network was yielded by averaging all individual matrices. The same density level of 18.5% to the CCM network was chosen as the threshold to binarize the group-level GC matrix. Those nodes with total-degree values of at least one standard deviation (SD) greater than the average total-degree of the network were identified as brain hubs.

We identified 27 hubs from the GC-derived directed network according to the total-degree, 13 (48.15%) of which were overlapped with those in the CCM network. These overlapped hubs were mainly located in the medial prefrontal, visual and lateral parietal cortices (Fig. S8 and Table S4).

Supplemental Figures

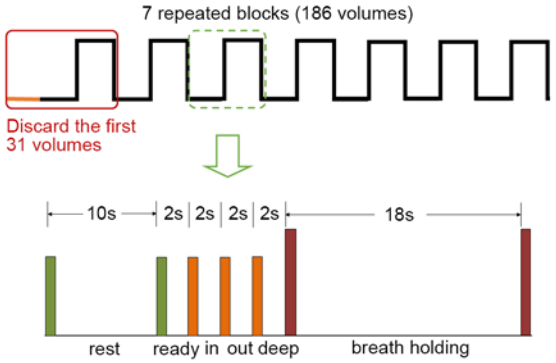

Figure S1. Brief description of the BH task design. During the T-fMRI scan, participants were required to perform a block-designed BH task with 7 repeated blocks (top). Within each block of 36 s, participants were instructed to keep rest for the first 10 s, then to get ready, breath in, breath out, deep breath for 2 s, separately, and finally to hold their breath for 18 s (bottom). During the data preprocessing, the 31 volumes before the 2nd block were discarded in analysis due to MRI signal equilibrium and subjects' adaptation to the task.

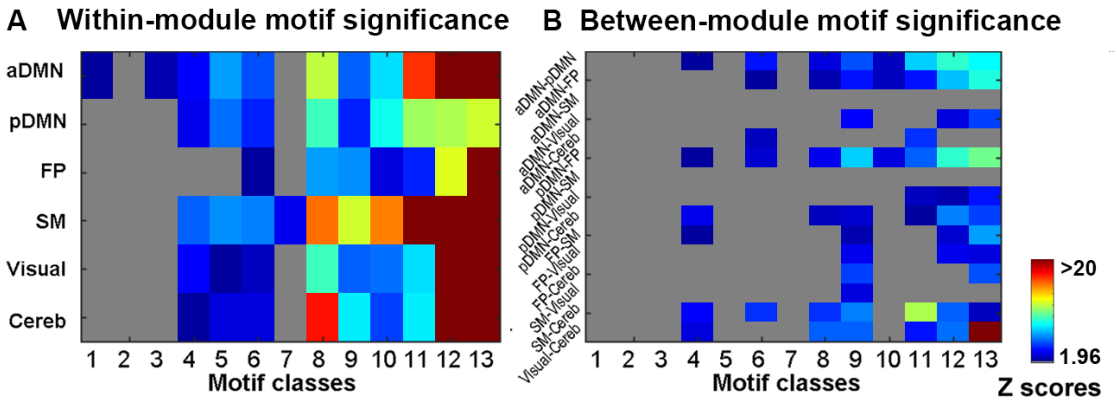

Figure S2. Within-/between-module three-node motif significance. Z scores were obtained by comparing motif count in the brain network to 100 stringent random networks conserving same number

of nodes, in-/out-degree, and number of unidirectional and reciprocal edges. Motif classes showing Z > 1.96 were defined as significant.

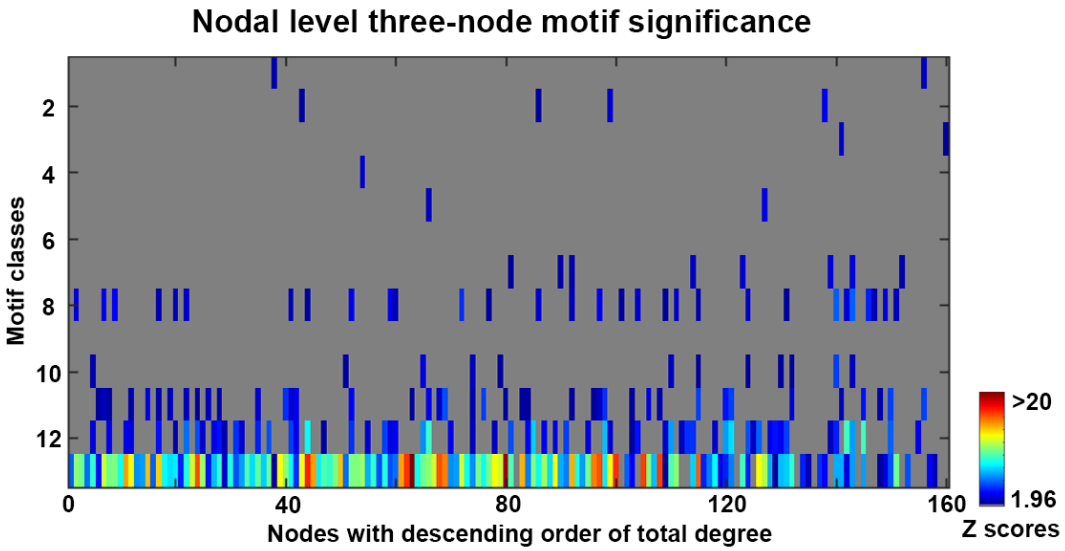

Figure S3. Nodal-level three-node motif significance. Z scores were obtained by comparing motif count in the brain network to 100 stringent random networks conserving same number of nodes, in-/out-degree, and unidirectional and reciprocal edges. Motif classes showing Z > 1.96 were defined as significant.

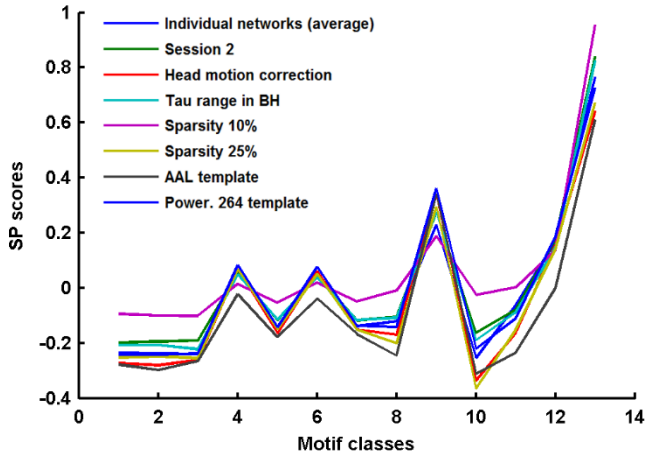

Figure S4. The significant profile (SP) curves of the three-node motifs in different validation analyses.

The profiles of SP curves were consistent across different validation cases.

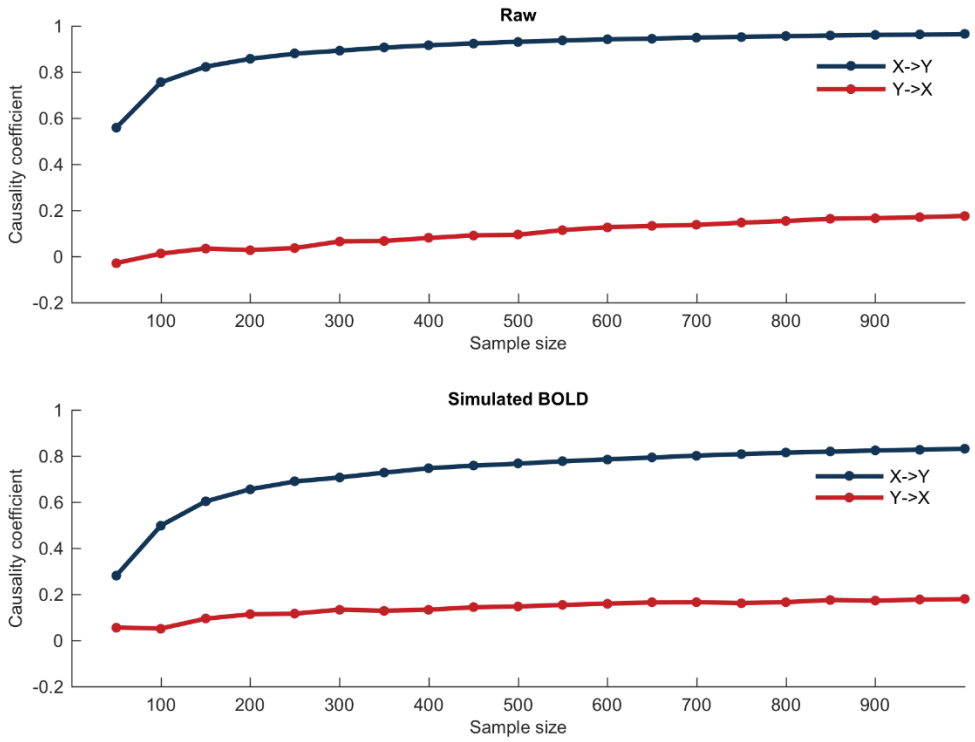

Figure S5. The relation between CCM predictability and data sample size. The simulation model contains two variables *X* and *Y*, where *X* causally affect *Y*, but not vice versa. The causality coefficients for *X* to *Y* increase with the increasing sample size, but reach a relative stability after sample size ≥ 200. The causality was estimated for the raw time series of the model (top panel) and the simulated BOLD signals (bottom panel). Blue line denotes the estimated average causality coefficient from X to Y. Red line denotes the estimated average causality coefficient from Y to X.

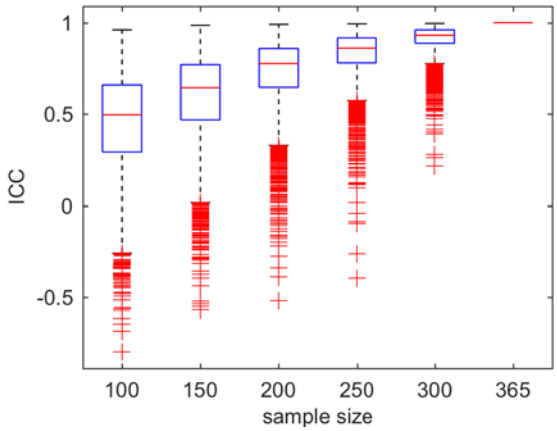

Figure S6. Edge-wise ICC between matrices at sample size 365 and lower sample size levels. The central mark of each box is the median, the edges of the box are the 25th and 75th percentiles, the whiskers extend to the most extreme data points not considered outliers.

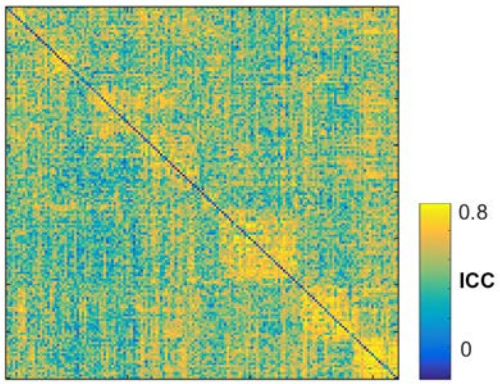

Figure S7. Edge-wise *ICC* across different E levels. 30.7% connections showed *ICC* > 0.8, and 96.9% connections exhibited *ICC* > 0.4.

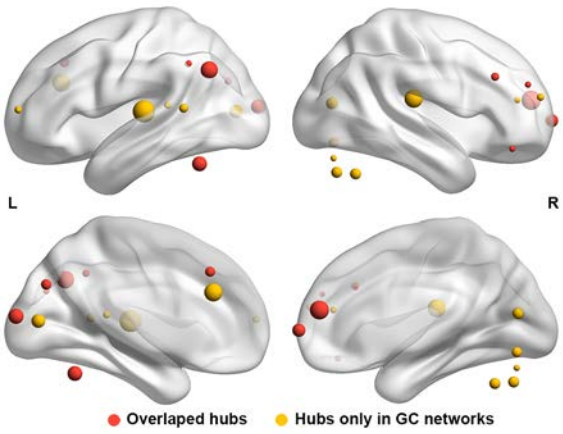

Figure S8. Total-degree Hubs in the GC derived functional brain network. Red: overlapping with the CCM-derived results in the main text. Yellow: non-overlapping hubs only identified in GC-derived network.

Supplemental Tables

Table S1. Demographic information of the participants

Subject ID	Gender	Age	Whether included in current study (if not, give reasons)
2475376	Male	21	included
9630905	Female	36	included
2799329	Male	30	included
8735778	Female	31	included
3808535	Male	25	included
7055197	Female	22	included
1427581	Female	27	included
3201815	Male	48	included
4176156	Male	46	included
3315657	Male	19	included
2842950	Male	27	excluded (unknown volumes in T-fMRI data)
21001	Male	57	excluded (brain atrophy)
3795193	Male	57	excluded (excessive head motion)
21006	Male	32	excluded (no diagnositic information)
21024	Male	22	excluded (no diagnositic information)
21018	Male	36	excluded (no diagnositic information)
21002	Male	52	excluded (no diagnositic information)
3893245	Male	38	excluded (psychiatric disease)
3313349	Female	22	excluded (psychiatric disease)
1961098	Female	21	excluded (psychiatric disease)
8574662	Male	42	excluded (psychiatric disease)
1793622	Male	60	excluded (psychiatric disease)
4288245	Male	22	excluded (psychiatric disease)
6471972	Male	32	excluded (psychiatric disease)

Table S2. Hub nodes of the directed functional brain network

Hub regions	MNI coordinates			IN degree	OUT degree	TOTAL degree	(IN-OUT) / TOTAL
Angular gyrus	-48	-63	35	64	54	118	0.08
Ventromedial prefrontal cortex	9	51	16	55	62	117	-0.06
Dorsolateral prefrontal cortex	46	28	31	58	56	114	0.02
Temporal	46	-62	5	71	42	113	0.26
Ventrolateral prefrontal cortex	46	39	-15	54	58	112	-0.04
Ventromedial prefrontal cortex	6	64	3	65	46	111	0.17
Anterior cingulate cortex	-1	28	40	50	58	108	-0.07
Medial prefrontal cortex	0	51	32	56	49	105	0.07
Occipital	-29	-75	28	51	51	102	0
Occipital	-16	-76	33	45	57	102	-0.12
Inferior parietal sulcus	-36	-69	40	57	43	100	0.14
Inferior parietal lobe	-48	-47	49	46	54	100	-0.08
Supplementary motor area	0	-1	52	49	51	100	-0.02
Temporoparietal junction	-52	-63	15	56	41	97	0.15
Anterior Prefrontal cortex	27	49	26	47	49	96	-0.02
Occipital	-2	-75	32	49	44	93	0.05
Dorsolateral prefrontal cortex	40	36	29	47	46	93	0.01
Anterior insula	38	21	-1	48	45	93	0.03
Post cingulate	1	-26	31	44	48	92	-0.04
Post occipital	-4	-94	12	50	41	91	0.10
Lateral cerebellum	-34	-57	-24	51	40	91	0.12
Ventral prefrontal cortex	42	48	-3	45	45	90	0
Parietal	-47	-18	50	45	45	90	0
Dorsolateral prefrontal cortex	-44	27	33	49	38	87	0.13
Superior frontal	-16	29	54	35	51	86	-0.19
Inferior cerebellum	-21	-79	-33	47	39	86	0.09
Inferior parietal lobe	-53	-50	39	38	47	85	-0.11

Table S3. Summary of the small-world architecture and whole-brain motif patterns in validations

Validation cases	Density	Small-worldness			two-node motifs		three-node motifs
		γ	λ	σ	unidirectional / reciprocal motif count	Z_{rand} (reciprocal motif)	significant motifs' ID ($Z > 1.96$)
In the text	**18.5%**	**1.61**	**1.03**	**1.56**	**1573 / 1568**	**61.8**	**4, 6, 9, 12, 13**
Individual networks	18.5% ±4.0%	1.28 ±0.13	1.02 ±0.02	1.25 ±0.13	1891±362/ 1409±360	44.3 ±3.54	4, 6, 9, 12, 13
Scanning session	17.8%	1.58	1.03	1.53	1493 / 1514	61.8	4, 6, 9, 12, 13
Head motion	24.6%	1.30	1.01	1.29	2049 / 2099	58.7	4, 6, 9, 12, 13
Tau range in BH	18.1%	1.58	1.03	1.53	1484/ 1560	56.0	4, 6, 9, 12, 13
Sparsity (0.10)	10.0%	2.81	1.12	2.5	702 / 921	63.2	4, 6, 9, 12, 13
Sparsity (0.25)	25.0%	1.3	1.01	1.28	2094 / 2133	69.5	4, 6, 9, 12, 13
Parcellation (AAL90)	34.9%	1.17	1.02	1.14	595 / 1098	38.3	9, 13
Parcellation (Power 264)	15.9%	1.34	1.02	1.31	4085 / 3468	85.9	4, 6, 9, 12, 13

Table S4. Hub nodes of the directed functional brain network derived by Granger causality analysis

Hub regions	MNI coordinates			IN degree	OUT degree	TOTAL degree	(IN-OUT) / TOTAL	Overlap with CCM network
Temporal	-54	-22	9	70	57	127	0.10	NO
Ventromedial prefrontal cortex	9	51	16	57	63	120	-0.05	YES
Post insula	42	-24	17	78	39	117	0.33	NO
Anterior cingulate cortex	-2	30	27	55	61	116	-0.05	NO
Angular gyrus	-48	-63	35	67	47	114	0.18	YES
Medial prefrontal cortex	0	51	32	87	26	113	0.54	YES
Post occipital	-4	-94	12	24	84	108	-0.56	YES
Lateral cerebellum	-34	-57	-24	30	77	107	-0.44	YES
Post occipital	-5	-80	9	46	58	104	-0.12	NO
Ventromedial prefrontal cortex	6	64	3	71	32	103	0.38	YES
Occipital	9	-76	14	50	50	100	0	NO
Inferior cerebellum	32	-61	-31	55	42	97	0.13	NO
Inferior cerebellum	33	-73	-30	54	43	97	0.11	NO
Occipital	-2	-75	32	57	38	95	0.20	YES
Medial cerebellum	5	-75	-11	21	74	95	-0.56	NO
Anterior cingulate cortex	-1	28	40	59	35	94	0.26	YES
Temporal	-59	-47	11	76	15	91	0.67	NO
Medial prefrontal cortex	0	15	45	33	57	90	-0.27	NO
Dorsolateral prefrontal cortex	46	28	31	52	37	89	0.17	YES
Anterior Prefrontal cortex	29	57	18	36	51	87	-0.17	NO
Anterior Prefrontal cortex	-29	57	10	60	27	87	0.38	NO
Temporal	-53	-37	13	57	30	87	0.31	NO
Inferior parietal lobe	-53	-50	39	56	30	86	0.30	YES
Ventrolateral prefrontal cortex	39	42	16	63	22	85	0.48	NO
Occipital	-29	-75	28	34	51	85	-0.20	YES
Ventrolateral prefrontal cortex	46	39	-15	43	41	84	0.02	YES
Anterior Prefrontal cortex	27	49	26	30	54	84	-0.29	YES
Medial cerebellum	14	-75	-21	44	40	84	0.05	NO

References

Buxton, R.B., Wong, E.C., Frank, L.R. (1998) Dynamics of blood flow and oxygenation changes during brain activation: the balloon model. Magn Reson Med, 39:855-64.

Erhardt, E.B., Allen, E.A., Wei, Y., Eichele, T., Calhoun, V.D. (2012) SimTB, a simulation toolbox for fMRI data under a model of spatiotemporal separability. Neuroimage, 59:4160-7.

Friston, K.J., Mechelli, A., Turner, R., Price, C.J. (2000) Nonlinear responses in fMRI: the Balloon model, Volterra kernels, and other hemodynamics. Neuroimage, 12:466-77.

Granger, C.W.J. (1969) Investigating Causal Relations by Econometric Models and Cross-spectral Methods. Econometrica, 37:424-438.

Kennel, M.B., Brown, R., Abarbanel, H.D.I. (1992) Determining Embedding Dimension for Phase-Space Reconstruction Using a Geometrical Construction. Phys Rev A, 45:3403-3411.

Landis, J.R., Koch, G.G. (1977) The measurement of observer agreement for categorical data. Biometrics, 33:159-74.

Shrout, P.E., Fleiss, J.L. (1979) Intraclass correlations: uses in assessing rater reliability. Psychol Bull, 86:420-8.

Sugihara, G., May, R., Ye, H., Hsieh, C.H., Deyle, E., Fogarty, M., Munch, S. (2012) Detecting causality in complex ecosystems. Science, 338:496-500.

Tajima, S., Yanagawa, T., Fujii, N., Toyoizumi, T. (2015) Untangling Brain-Wide Dynamics in Consciousness by Cross-Embedding. PLoS Comput Biol, 11:e1004537.